Journal of Statistical Physics, Vol. 88, Nos. 5/6, 1997

On the Stability of Time-Harmonic Localized States in a Disordered Nonlinear Medium

Jared C. Bronski,[1] David W. McLaughlin,[2] and Michael J. Shelley[2]

Received August 30, 1996; final April 30, 1997

We study the problem of localization in a disordered one-dimensional nonlinear medium modeled by the nonlinear Schrödinger equation. Devillard and Souillard have shown that almost every time-harmonic solution of this random PDE exhibits localization. We consider the temporal stability of such time-harmonic solutions and derive bounds on the location of any unstable eigenvalues. By direct numerical determination of the eigenvalues we show that these time-harmonic solutions are typically unstable, and find the distribution of eigenvalues in the complex plane. The distributions are distinctly different for focusing and defocusing nonlinearities. We argue further that these instabilities are connected with resonances in a Schrödinger problem, and interpret the earlier numerical simulations of Caputo, Newell, and Shelley, and of Shelley in terms of these instabilities. Finally, in the defocusing case we are able to construct a family of asymptotic solutions which includes the stable limiting time-harmonic state observed in the simulations of Shelley.

KEY WORDS: Nonlinear Schrödinger equation; random media.

1. INTRODUCTION

The phenomena of localization was first studied in condensed matter physics as a model for the conduction/insulation of electrons in disordered lattices. In a *periodic* lattice a single electron is governed by the Schrödinger equation,

$$i\psi_t = -\psi_{xx} + U(x)\,\psi$$

where the *periodic* potential $U(x)$ represents the underlying lattice. The spectrum of such a Schrödinger operator consists of bands of continuous

[1] Department of Mathematics, Stanford University, Stanford, California 94305.
[2] Courant Institute of Mathematical Sciences, New York, New York 10012.

0022-4715/97/0900-1077$12.50/0

822/88/5-6-6

spectrum separated by gaps, with no point spectrum (Bloch's theorem). This implies that, as in the case of the free Schrödinger equation, the variance of an initial wave-packet will grow quadratically in time:

$$\langle x^2 \rangle - \langle x \rangle^2 \propto t^2 \qquad \text{where} \quad \langle \cdot \rangle = \int (\cdot)\, \psi \psi^* \, dx$$

In 1958 Anderson[1] discovered a striking result: If the periodic Schrödinger problem is perturbed by the addition of a random potential $V(x, \omega)$ of any amplitude,

$$i\psi_t = -\psi_{xx} + U(x)\, \psi + V(x, \omega)\, \psi$$

then an initially localized wavepacket will remain localized for all time, and true wave propagation does not take place. More precisely, a wave packet evolving in any one-dimensional disordered medium has a variance which grows strictly slower than quadratically for large times,

$$\frac{\langle x^2 \rangle - \langle x \rangle^2}{t^2} \to 0, \qquad \text{as} \quad t \to +\infty$$

This was later proven by Fröhlich and Spencer,[2] who showed exponential decay of the Green's function. This implies[3] the absence of absolutely continuous spectrum. It was later shown that the spectrum of the random Schrödinger operator has only pure point spectrum.[4–8] For the scattering problem, this implies that the transmission coefficient decays to zero exponentially with the length of the medium.

The phenomena of localization in linear systems is so striking both mathematically and physically that it is compelling to ask whether it persists in the presence of nonlinearities.[9–13, 8, 14, 15] The nonlinear Schrödinger (NLS) equation,

$$i\psi_t = -\psi_{xx} + V(x)\, \psi + \beta\, |\psi|^2\, \psi,$$

is a canonical equation which describes nearly monochromatic, weakly nonlinear and strongly dispersive classical waves. In this framework of nonlinear waves, it is natural to consider the additional effects of a random inhomogeneity. Furthermore, the random NLS equation might also be relevant in a quantum setting, as a Hartree–Fock or mean-field approximation to a large number of quantum particles in a common (random) potential interacting with each other via a delta function interactions. This potential quantum application is considered in Ref. (16).

The central issue is the competition between nonlinear and random effects. In the absence of a potential $V(x, \omega)$, the random NLS equation reduces to the cubic Schrödinger equation, which is integrable by the Inverse Scattering Transform, and has very different behavior depending upon the sign of β ($\beta < 0$ – a focusing medium, $\beta > 0$ – a defocusing medium). In the absence of nonlinearity ($\beta = 0$), we have a one-dimensional Schrödinger equation with a random potential, as discussed above.

Previous work has considered the combined effects of nonlinearity and randomness. Devillard and Souillard[10] have shown that a class of time-harmonic solutions to the random nonlinear Schrödinger equation exhibits localization. They show further that the decay of a transmission coefficient is slower than exponential. Knapp, Papanicolaou, and White[11, 17] have made a detailed study of the time-harmonic, random NLS equation subject to two-point boundary conditions. In this situation, solutions to this boundary value problem are not unique, and they find that the multiplicity of solutions tends to *inhibit* localization. Note that these two studies are not in conflict, as they consider different boundary conditions. Doucot and Rammal[8] consider the problem of localization in a random NLS equation by using invariant imbedding techniques. Finally, we refer the reader to the survey article of Gredeskul and Kivshar.[14] All of these works are concerned primarily with time-harmonic solutions to the random NLS equation. Such solutions have interesting properties, but the question of their stability is open. The stability of such solutions will be a major thrust of this paper.

In this paper we present a study, for the random NLS equation, of the competition between nonlinearity and randomness, and the effects of this competition upon localization. We focus specifically on nonlinear states and their linear instabilities as mechanisms for the destruction of localization. This general study uses numerical simulation, together with formal asymptotic calculations and some mathematical analysis, to unveil qualitative properties of the delocalized field—qualitative properties that are distinct in focusing and defocusing media.

The paper is structured as follows: In Section 2, the fixed input and fixed output boundary value problems are defined, and the results of Devillard and Souillard on the fixed output problem are briefly summarized. In addition, numerical results and observations on the fixed output problem are presented. In Section 3, a synopsis is given of the numerical results of Caputo, Newell, and Shelley,[9] and of Shelley[18] for the fully time-dependent random NLS equation. These numerical simulations show that localized time-harmonic solutions are not those actually observed, suggesting that such time-harmonic solutions are unstable. In Section 4, we consider the linearized stability of time-harmonic solutions,

which is governed by a non-self-adjoint eigenvalue problem, and derive bounds on the locations of unstable eigenvalues in the complex plane. In Section 5, we solve this eigenvalue problem numerically, and find generically that these solutions are indeed unstable. By computing the spectra for many realizations of the random potential, we are able to find the distribution of eigenvalues in the complex plane—distributions that are distinct for focusing and defocusing nonlinearities. We also argue that the instabilities are connected to resonances in the Schrödinger equation, and relate these instabilities to the phenomena observed by Shelley. Finally we construct asymptotic solutions which reproduce long-time behavior seen in some of the numerical experiments of Shelley. Section 6 gives concluding remarks.

2. THE FIXED OUPUT PROBLEM

In this section we formulate a problem in nonlinear localization, adopting the approach taken by Devillard and Souillard.[10] First, we review their results for the time-harmonic fixed output problem. Then, we describe some numerical solutions of this problem that display several interesting new features of nonlinear localization.

Localization is very well understood for the linear case,[1, 4–6]

$$i\psi_t = -\psi_{xx} + V(x, \omega)\,\psi$$

with $V(x, \omega)$ random (the specific random potentials will be defined below). This problem can be understood by studying the time-independent spectral problem

$$E\psi = -\psi_{xx} + V(x, \omega)\,\psi \tag{1}$$

It can be shown[4, 6, 5, 7] that for almost every realization of the potential the eigenvalue problem Eq. (1) has

(i) Only pure point spectrum.

(ii) Exponentially decaying eigenfunctions.

In a nonlinear problem it is not clear *a priori* what is meant by localization. Obviously a characterization in terms of the spectrum ceases to have any meaning in the nonlinear case, since superposition no longer holds. There are many possible ways to define nonlinear localization, but we follow the convention adopted by Devillard and Souillard.[10]

Devillard and Souillard consider the time-harmonic scattering problem

$$\begin{aligned} \psi(x, t) &= \exp(-ik^2 t)\, F(x) \\ k^2 F &= -F_{xx} + V(x, \omega)\, F + \beta\, |F|^2\, F \end{aligned} \tag{2}$$

where $k^2 > V_{\max}$. They take the random potential $V(x, \omega)$ to be piecewise constant, with the length of each constant interval chosen from a Poisson distribution and the height chosen from a uniform distribution which is independent and identically distributed on each constant interval. The potential V is taken to consist of a finite number of such segments, so that V is compactly supported, say on $[0; L]$. The nonlinearity is also taken to be supported on $[0, L]$. Since the potential and nonlinearity are of compact support the solutions outside of $[0, L]$ are plane waves:

$$\begin{aligned} \psi(x) &\to T \exp(i(kx - k^2 t)) + S \exp(-i(kx + k^2 t)) \qquad x > L \\ \psi(x) &\to I \exp(i(kx - k^2 t)) + R \exp(-i(kx + k^2 t)) \qquad x < 0. \end{aligned}$$

The second-order ODE requires two boundary conditions to determine a solution. There are two distinct types of boundary value problems which are commonly studied:

(i) *Fixed Input* $I = 1$, $S = 0$.

(ii) *Fixed Output* $T = 1$, $S = 0$.

The fixed input boundary value problem is the more physical, corresponding most closely to the intuitive picture of scattering. It amounts to sending in a plane wave of fixed intensity and observing what is reflected and what is transmitted. (This is the boundary value problem studied by Knapp, Papanicolaou, and White.[11, 17]) This fixed input problem is a nonlinear two-point boundary value problem that does not necessarily have a unique solution. This is expected, since even very simple boundary value problems can exhibit multi-stability and non-uniqueness of solutions. On the other hand, the fixed output problem is an initial value problem in x, and has a unique solution. This makes it a much easier problem to study both numerically and analytically. [This is the boundary value problem studied by Devillard and Souillard.] In either case, the transmission coefficient is defined as

$$t_L = \frac{T}{I}$$

The transmission coefficient is a function of L, the length of support of the disordered medium. Localization is taken to mean that $t_L \to 0$ as $L \to \infty$.

The linear case—where the two boundary value problems are equivalent—can be treated by a transfer matrix formalism,[19] from which it is well-known that the transmission coefficient decays exponentially:

$$t_L \propto \exp(-\gamma L), \qquad L \gg 1$$

Here the inverse "localization length," $\gamma = \gamma(k)$, is a decay constant which depends on the random medium and the wavenumber k of the incident plane wave.

In their study of the fixed output problem, Devillard and Souillard show that for the nonlinear problem, the transmission coefficient t_L decays to 0 as L goes to infinity, establishing localization. They show further that in the cubic focusing case:

$$t_L \geqslant CL^{-2}, \qquad L \gg 1$$

Thus, the decay is *no faster* than algebraic, and certainly not exponential as in the linear case. Using a heuristic argument with supporting numerical evidence they suggest the improved estimate

$$t_L \propto L^{-1}, \qquad L \gg 1$$

Their approach is quite general, and extends to many different nonlinearities. Further it is an analytical work and not, (for instance) perturbative, Their argument that the decay of t_L is slower than exponential appears to hold only for a focusing nonlinearity. It is also important that, in the linear problem, a complete understanding of the time-harmonic eigenvalue problem leads, through the Fourier transform, to a complete understanding of the dynamic problem. As Devillard and Souillard point out this is no longer true in the nonlinear case, due to the failure of superposition, and that an understanding of the time-harmonic problem does not allow one to understand the dynamical problem. The time-harmonic problem says nothing, for example, about the rate of spreading of an initially localized wavepacket, nor does it address the question of the stability of the localized solutions which are constructed.

To sharpen our understanding of the work of Devillard and Souillard, we have performed numerical experiments on the fixed output problem, Eq. (2). We begin by generating a random potential by the method outlined in the next paragraph. We impose initial conditions at the edge of the medium, $x = 500$, corresponding to an outgoing plane wave. We then integrate the random, time-harmonic NLS equation back to the beginning of the medium, $x = 0$, using a standard fourth order Runge–Kutta scheme. We repeat this procedure for many (≈ 4000) realizations of the random

potential $V(x, \omega)$, and calculate the average amplitude of the wave as a function of distance into the medium. The medium was (for each realization) discretized into 4096 points, giving $\Delta x \approx \cdots 12$.

The random potential $V(x, \omega)$ was generated in the following manner: At each spatial gridpoint a random value was chosen from a uniform distribution to generate a very rough random potential—one with a correlation length on the grid scale. This rough potential was then smoothed by convolution with a smooth kernel $\operatorname{sech}(x/x_c)$ to give a random potential with a characteristic correlation length x_c. The correlation length x_c of the random potential was 2, so that the disordered medium was approximately 250 correlation lengths long.

The incident wavenumber k and the maximum height of the random potential V were chosen to be unity, so that $k^2 - V(x) \geqslant k^2 - 1 \geqslant 0$. Thus there are no classically forbidden regions, and any observed decay of the solution is due to localization, rather than the exponential decay associated with tunnelling. For the nonlinear case the coefficient of the (focusing) nonlinearity was $\beta = -0.25$.

It should also be pointed out that the arguments used by Devillard and Souillard to bound the decay rate of the transmission coefficient are quite robust, and are easily extended to (for instance) bounded random potentials, as we simulate here. Thus we felt justified in simulating a potential which does not correspond exactly to the one chosen by Devillard and Souillard. In the linear case localization phenomena tend to be rather robust, and do not depend too much on the exact nature of the random potential, and thus it is hoped that the same hold true in the nonlinear problem. The numerics which follow tend to support this, as we observe numerically the same phenomena which were theoretically predicted and numerically verified by Devillard and Souillard.

These experiments are summarized in Fig. 1a, b, which show the average wave amplitude as a function of distance into the medium, for both the linear and focusing nonlinear cases. There is a dramatic difference between the linear case, where we see exponential decay of the solution, and the nonlinear case, where we see a decay which is much slower. The linear case requires an incident wave of average amplitude roughly 900 to produce a transmitted wave of unit amplitude, while the nonlinear case requires an incident wave of amplitude roughly 1.8 to achieve the same transmission. This is a *striking* reduction in the reflectivity of the medium!

It is also very interesting to examine, for the linear and nonlinear cases, the reflection coefficient (defined as $r_L = R/I$) as a function of the incident wavenumber k. (This experiment is, to our knowledge, new, and has not appeared in any previous work on random nonlinear media.) To this end we performed a series of numerical experiments for a *single*

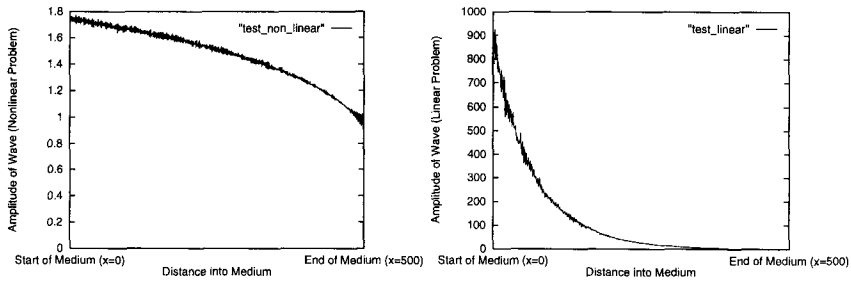

(a) Nonlinear Medium (b) Linear Medium

Fig. 1. Average Amplitude of Wavefunction vs. Distance into the Medium.

realization of the random potential, but for a range of incident wavenumbers. This was repeated for three different widths of the disordered medium ($L = 200$, 400, 800). The results of these experiments are summarized in Figs. 2 and 3. In Fig. 2, the graphs on the left show r_L as a function of k for the linear problem, while those on the right show r_L for the nonlinear problem. It is apparent that in the nonlinear problem the chance of having a "resonant" transmission is much greater. This is seen in the enormous amount of small scale structure in the nonlinear reflection coefficient. In the case of small k, for instance, most of the medium is a classically forbidden region, and the wave function must tunnel through the medium. Thus the linear reflection coefficient is essentially unity, with a few isolated resonances where the reflection coefficient is less than one. The nonlinear reflection coefficient, on the other hand, shows an extremely large number of such resonances.

There also appears to be a qualitative difference between the oscillatory structure of the linear and nonlinear reflection coefficients as a function of the wavenumber k. To see this difference, first consider Figs. 2e and f, which show dense oscillations for a medium of length $L = 800$, over a range in k from 0 to 4. Fig. 3 shows successively smaller details of Figs. 2e and f—$k \in [2, 2.25]$ and $k \in [2.12, 2.13]$. It becomes apparent that, when viewed on a scale where the linear reflection coeffficient appears smooth, the nonlinear reflection coefficient still remains very irregular and highly oscillatory (though with isolated, smooth "islands").

In general, we have observed that for small wavenumber k, the "islands" of smooth behavior in r_L for the nonlinear problem are quite small and sparse, and wild fluctuations seem to be the norm. For larger k, r_L appears instead to be quite smooth, and looks very much like that for the linear problem under a slight shift in wavenumber. It isn't difficult to argue that for *fixed* L and *large* k, the reflection coefficient for the

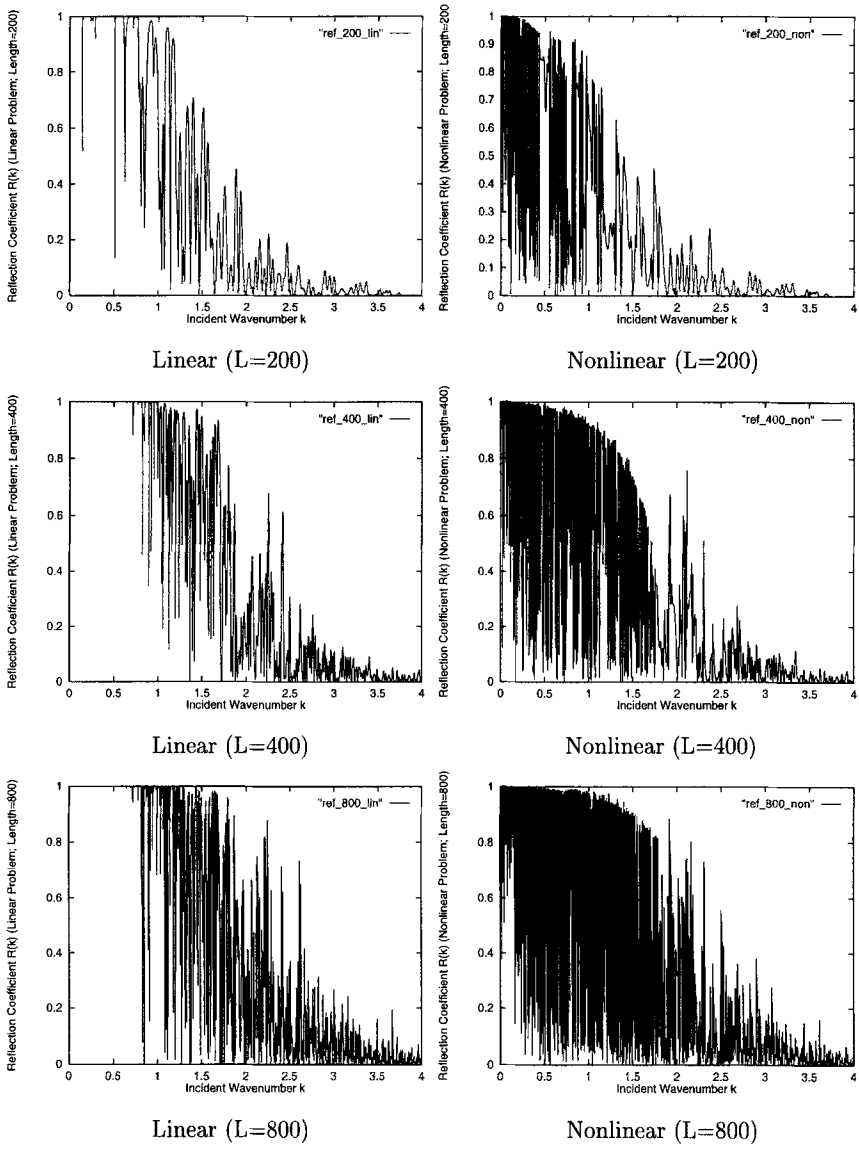

Fig. 2. Reflection Coefficients vs. Wavenumber for linear (Left) and Nonlinear (Right) Problems.

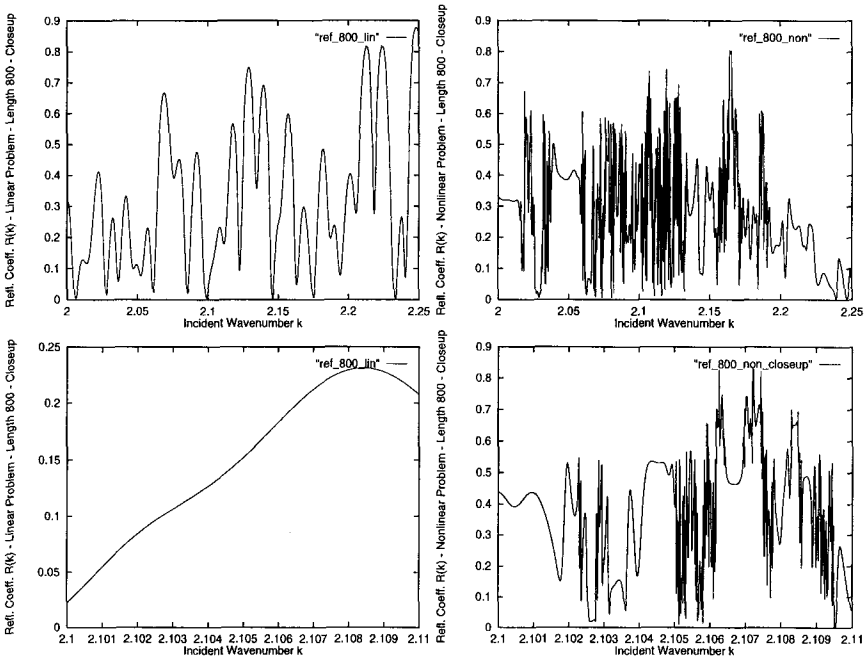

Fig. 3. Details of Linear and Nonlinear Reflection Coefficients.

nonlinear problem, r_L^{nl} should be related to the reflection coefficient for the linear problem, r_L^l, by

$$r_L^{nl}(k) \approx r_L^l((k^2 + |A|^2)^{1/2})$$

where $|A|$ is the amplitude of the incident plane wave. This is well supported by our numerical data.

It is tempting to speculate that the wild behavior of the reflection coefficient in the fixed output problem is related to the nonuniqueness of solutions to the fixed input problem,[11] with those values of k for which the fixed output problem exhibits wild behavior corresponding to values of k for which the fixed input problem exhibits a large multiplicity of solutions. This would be an interesting area for a future study.

3. PREVIOUS NUMERICAL RESULTS

In this section we summarize previous numerical results of Caputo, Newell, and Shelley[9] and of Shelley[18] on the fully time-dependent random NLS scattering problem.

These works consider the discrete random NLS equation

$$i\psi_t^n = -(\psi^{n+1} - 2\psi^n + \psi^{n-1}) + V_n(\omega)\,\psi^n + \beta\,|\psi^n|^2\,(\psi^{n+1} + \psi^{n-1})$$

with absorbing boundary conditions and initial conditions corresponding to a plane wave incident from negative infinity. This particular discretization was chosen because it is completely integrable in the absence of an external potential.[20] The incident wavenumber k was chosen so that the kinetic energy k^2 is slightly larger than the maximum height of the random potential V_n. This is physically the most interesting situation. The case where k^2 is very small corresponds to a case where classically there should be no transmission. In such a situation localization is somewhat uninteresting. On the other hand if the kinetic energy k^2 is much larger than the size of the random potential then one can only observe localization phenomena over large spatial scales, which makes the problem numerically difficult and computationally expensive. In short the interesting regime is the one where the kinetic energy of the incident plane wave, the height of the random potential and the size of the nonlinearity are all of comparable size, and all of these effects are important.

The random potential was generated by the following algorithm. A random number was chosen at each site from a uniform distribution $V_n \in [0, 1]$, producing a very rough random potential. This random potential was then smoothed by convolving it with a smoothing function with some characteristic lengthscale, chosen to be large compared with the lattice spacing but small compared with the incident wave-length k^{-1}. The absorbing boundary conditions were simulated by giving the potential a small negative imaginary part supported near the boundaries. This has the effect of causing exponential decay (in time) of waves near the boundaries. The ODE's themselves were integrated with a fourth order Runge–Kutta ODE solver. Some of Shelley's numerical results are summarized in Figs. 4–6.

Figure 4 shows a single realization of the random potential, which was generated according to the above algorithm. Figs. 5a–c depict the long-time amplitude profiles for the linear, focusing, and defocusing problems. In each of these cases the absorbing layer is supported near the edges of the medium, from $n = 0$ to 50 and from $n = 450$ to 500. The nonlinearity and the random potential are supported from $n = 100$ to 400. In the region between the support of the random medium and the support of the absorbing layer the waves propagate freely (according to the linear Schrödinger equation with no potential).

Figure 5a shows the solution to the linear problem with a plane wave incident from left-hand edge of the medium, after a sufficiently long time

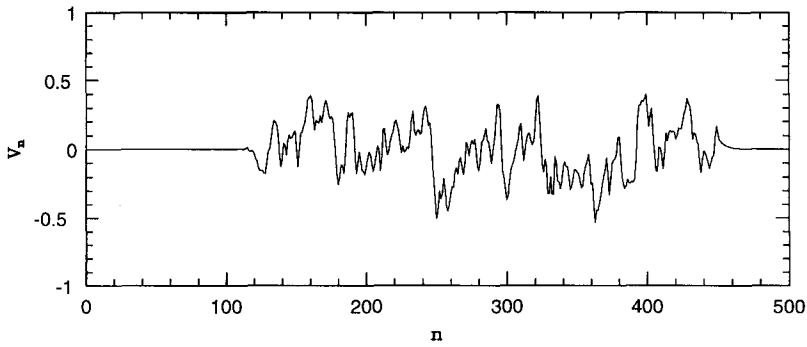

Fig. 4. Random Potential (after smoothing).

that initial transients have died away. At the left hand edge of the graph (in the absorbing layer) we see the incident plane wave, with amplitude $|A| \approx .04$. In the region between $n = 50$ and 100, in the segment between the absorbing layer and the medium, the amplitude of the wavefunction oscillates between $|A| \approx 0$ and $|A| \approx 0.08$. These oscillations are due to interference between the incident plane wave and the reflected plane wave, which are of roughly the same amplitude, and indicates that nearly all of the incident beam is being reflected. Within the medium the amplitude decays in what seems to be an exponential fashion. This is the hallmark of linear localization. By averaging many realizations Shelley was able to observe a clear exponential decrease in the transmitted signal. In the far field, from $n = 400$ to 450 the amplitude is very small, indicating that very little of the incident beam is being transmitted. The transmitted beam is dissipated in the absorbing layer between $n = 450$ and 500.

Figure 5b shows the long-time amplitude profile for the focusing problem, in the solid line, together with the background potential, in the dashed line. The amplitude profile for the problem with a focusing nonlinearity appears markedly different from that of the linear problem. In the focusing case the profile is dominated by relatively large amplitude, narrow spikes which are bound to local minima of the background potential. The amplitudes of these soliton-like structures are far greater than the amplitude of the incident beam. Note in particular that this solution looks nothing like the time harmonic solutions shown in Fig. 1 of the previous section. Shelley also found the time spectrum to be extremely non-monochromatic, since each soliton has its own frequency of oscillation, thus violating the time harmonicity assumptions. These observations suggest that time-harmonic solutions are not those that are physically observed for the focusing nonlinearity.

It is somewhat unclear how to interpret this result as localization, or lack thereof. The definition of localization in terms of the decay of the

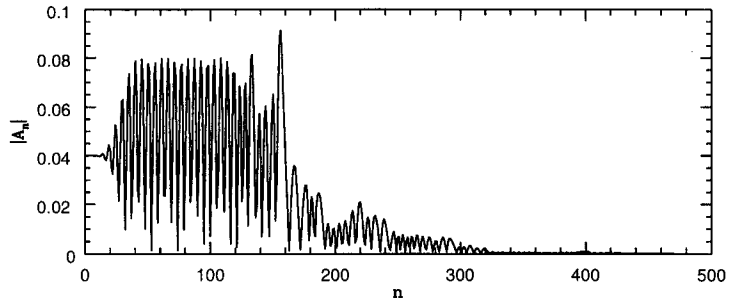

Solution to the Linear Problem

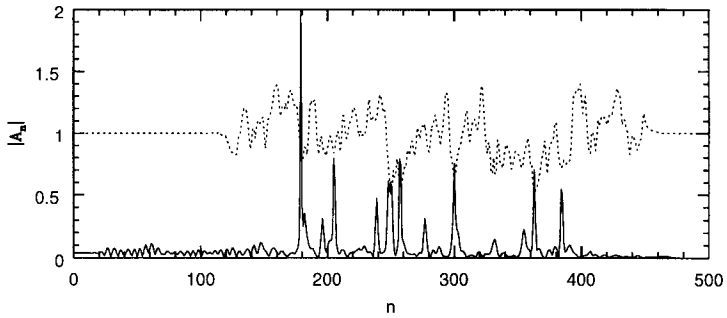

Solution to the Focusing Problem (with superimposed potential)

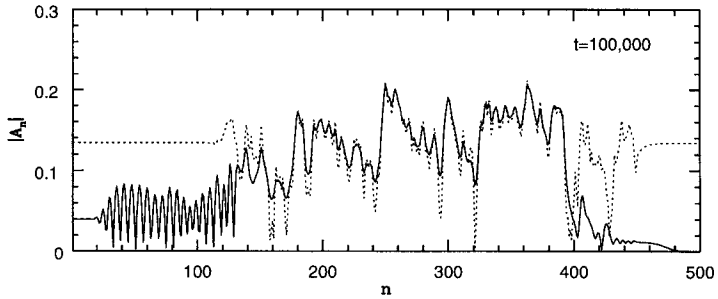

Solution to the Defocusing Problem (with superimposed potential)

Fig. 5. Solutions to the Linear, Focusing and Defocusing Problems.

transmission coefficient adopted by Devillard and Souillard is not applicable to this problem, since the long time state appears to have non-trivial dynamical behavior in time. The numerical evidence suggests that these bound solitons can arise at any distance into the medium, which in turn suggests that the long time state is not localized, since at long times there is field

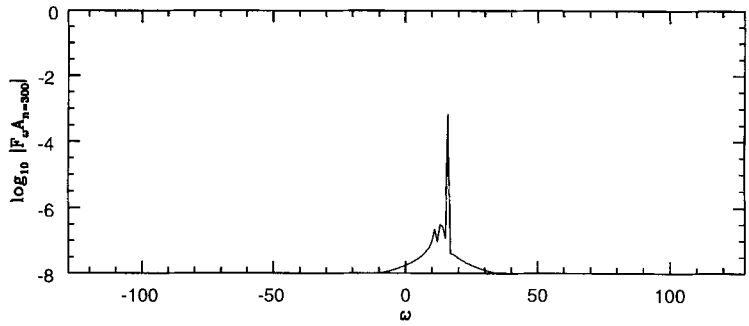

Fig. 6. Frequency Spectrum of the Defocusing Problem.

supported arbitrarily deeply in the disordered media. However we stress that more numerics, as well as a definition of localization which applies to the fully time-dependent case, are necessary to fully resolve this question.

The third and arguably the most interesting case is shown in Fig. 5c, which shows the long-time amplitude of the nonlinear defocusing problem, in the solid line, along with the background potential, drawn in the dashed line. This solution shows neither decay, as in the linear case, nor development of tightly localized structures, as in the focusing case. What is observed is that $|\psi|^2$ is spread rather uniformly throughout the support of the medium, and the amplitude within the medium is markedly greater than the input amplitude. Shelley observed that at long times the amplitude of the wavefunction $\beta |\psi|^2$ satisfies the approximate equality

$$\beta |\psi|^2 (x) \approx k^2 - V(x)$$

indicating a lack of localization. This approximate equality is evident in Fig. 5c. It is interesting to note that after an initial transient, the frequency settles down to being nearly monochromatic. This is apparent from Fig. 6, which shows the frequency spectrum (in time) of a point in the center of the slab. This spectrum has most of its energy in the incident frequency. Since Devillard and Souillard have shown that almost every time-harmonic solution of the fixed output problem is localized, it appears that the dynamics has acted to select an *atypical* delocalized time-harmonic solution.

4. THE STABILITY OF TIME-HARMONIC SOLUTIONS

We consider a random nonlinear medium as described by the random NLS equation

$$i\psi_t = -\psi_{xx} + V(x, \omega)\, \psi + \beta |\psi|^2 \psi \tag{3}$$

within the support of the medium, ($x \in [0, L]$), and the free Schrödinger equation

$$i\psi_t = \psi_{xx}$$
$$\psi \to T \exp(ikx) \qquad x \to -\infty$$
$$\psi \to I \exp(ikx) + R \exp(-ikx) \qquad x \to -\infty$$

outside of the support of the medium. We recall from Section 2 that this equation supports time harmonic solutions $\psi(x, t) = F(x) \exp(-ik^2 t)$, which satisfy the ODE

$$k^2 F = -F_{xx} + V(x, \omega) F + \beta |F|^2 F$$

Under fixed output boundary conditions,

$$F'(L) - ikF(L) = 0$$

the above ODE becomes an initial value problem in x. For the focusing nonlinearity, $\beta < 0$, the solution to the above ODE exists and is unique. Introducing the energy $H = 1/2(k^2 |F|^2 + |F_x|^2 - \beta/2 |F|^4)$, which satisfies $H_x = V(x, \omega) \bar{F} F_x$, it is easy to show using positive definiteness of this energy, that

$$H_x = V(x, \omega) \bar{F} F_x$$
$$|H_x| \leqslant |k^{-1}| \, |V(x, \omega)| \, |kFF_x|$$

Since $|ab| \leqslant 1/2(a^2 + b^2)$ this gives

$$|H_x| \leqslant 1/2 \, |k^{-1}| \, |V(x, \omega)| \, (k^2 |F|^2 + |F_x|^2) \leqslant 1/2 \, |V(x, \omega)| \, |H|$$

Therefore H, and thus F and F_x, are bounded if V is a function which is absolutely integrable. This is similar to the argument used by Devillard and Souillard to bound the growth rates of F, and thus derive a bound on the decay of the transmission coefficient.

However for the defocusing case, $\beta > 0$, the solution may develop poles at finite values of x. This is easiest to see by considering the case $k = 0$, $V(x, \omega) = 0$. The resulting ODE is then given by

$$F_{xx} = |F|^2 F$$

which has the exact solution $F(x) = (2)^{1/3} (x - x_0)^{-1}$. For the defocusing case the energy H is unbounded below, and the bounds sketched above

collapse. For this reason it is necessary to consider nonlinearities which are more regular. Throughout this paper we consider the defocusing nonlinearity

$$N(F) = \beta |F|^2 F(1 + \beta |F|^2)^{-1}$$

The energy associated with this nonlinearity is bounded below.

It was shown by Devillard and Souillard that solutions to this ODE (under fixed output boundary conditions) are algebraically localized. The numerical solutions presented in the previous section, on the other hand, suggest that solutions of the fully time-dependent problem *do not* exhibit localization. These two observations, taken together, suggest that time-harmonic solutions to the random NLS are unstable, and thus are unlikely to actually be observed. This is further supported by the fact that in the absence of a potential the time-harmonic plane-wave solutions of focusing NLS are known to be unstable.

For these reasons we consider the stability of time-harmonic solutions to linear perturbation. In this section we derive bounds on the possible location of any unstable eigenvalues. Though these analytical bounds admit the possibility of instabilities, they do not establish their existence. In Section 5 we compute the time-harmonic soultions numerically, and establish the existence of instabilities with specific algorithms discussed in Section 5.

Let F denote a fixed time-harmonic solution, and introduce a small perturbation ϕ, defined by

$$\psi(x, t) = \exp(-ik^2 t)[F(x) + \varepsilon\phi(x, t)]$$

Substituting into Eq. (3), and collecting leading order terms in ε gives the following linearized equations for ϕ and $\bar{\phi}$:

$$\begin{aligned} i\phi_t + k^2\phi &= -\phi_{xx} + V(x)\,\phi + 2\beta |F|^2 \phi + \beta F^2 \bar{\phi} \\ -i\bar{\phi}_t + k^2\bar{\phi} &= -\bar{\phi}_{xx} + V(x)\,\bar{\phi} + 2\beta |F|^2 \bar{\phi} + \beta \bar{F}^2 \phi \end{aligned} \tag{4}$$

This definition for ϕ is convenient because the resulting linearized equations do not explicitly involve time. Rewriting in terms of the "sideband" variables f and g, defined by

$$\phi = f(x) \exp(-iEt) + \bar{g}(x) \exp(i\bar{E}t),$$

the stability problem becomes

$$\begin{aligned} Ef &= -k^2 f - f_{xx} + V(x)\, f + 2\beta\, |F|^2 f + \beta F^2 g \\ -Eg &= -k^2 g - g_{xx} + V(x)\, g + 2\beta\, |F|^2 g + \beta \bar{F}^2 f \end{aligned} \tag{5}$$

This is an eigenvalue problem for (E, f, g), where instability corresponds to $Im(E) > 0$. The allowable perturbations are those which do not change the asymptotic boundary conditions, and thus we only consider perturbations which are decaying at spatial infinity. This amounts to considering the above equation with L_2 boundary conditions.

Since we are interested in instability we need consider only eigenvalues with $Im(E) > 0$. Further we need only consider eigenvalues with positive real part since the above eigenvalue problem is invariant under the transformation

$$\begin{aligned} f(x) &\to \bar{g}(x) \\ g(x) &\to \bar{f}(x) \\ E &\to -\bar{E} \end{aligned}$$

The eigenvalue problem (5) is a pair of Schrödinger equations with a nonself-adjoint coupling. In the absence of this coupling, the equations reduce to

$$\begin{aligned} Ef &= -k^2 f - f_{xx} + V(x)\, f + 2\beta\, |F|^2 f \\ -Eg &= -k^2 g - g_{xx} + V(x)\, g + 2\beta\, |F|^2 g \end{aligned} \tag{6}$$

whose spectrum is easily understood. The spectrum of f consists of:

(i) Continuous spectrum for $E \geqslant -k^2$.

(ii) A finite number of bound states in $-k^2 + (V + 2\beta\, |F|^2)_{\min} \leqslant E \leqslant -k^2$.

The spectrum of g is the mirror image of that of f, namely:

(i) Continuous spectrum for $E \leqslant k^2$.

(ii) A finite number of bound states in $k^2 - (V + 2\beta\, |F|^2)_{\min} \geqslant E \geqslant k^2$.

(See Fig. 7)

The uncoupled problem has no instabilities (complex eigenvalues) since it is self-adjoint. Any instabilities must arise as a result of the non-self-adjoint coupling. We can bound both the magnitude of the imaginary part

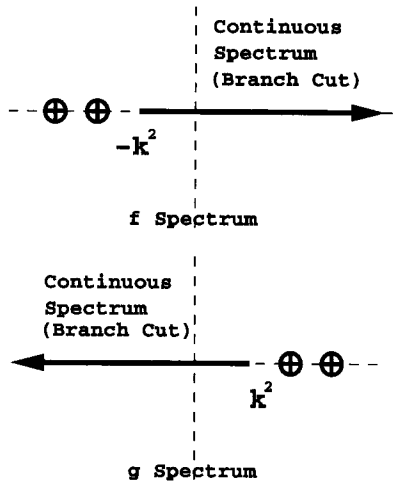

Fig. 7. The Spectrum of the Uncoupled Problem.

of the eigenvalues, and the real part of those eigenvalues which have a non-vanishing imaginary part. The spectrum of the eigenvalue problem given in Eq. (5) is characterized in the following theorem.

Theorem. The eigenvalue problem defined by Eq. (5) has the following properties:

(i) It is invariant under the transformation $(E, f, g) \to (-\bar{E}, \bar{g}, \bar{f})$.

(ii) The continuous spectrum $\sigma_{\text{cont.}}$ is the entire real axis.

(iii) The complex eigenvalues lie in a bounded region D of the complex plane, shown schematically in Fig. 8.

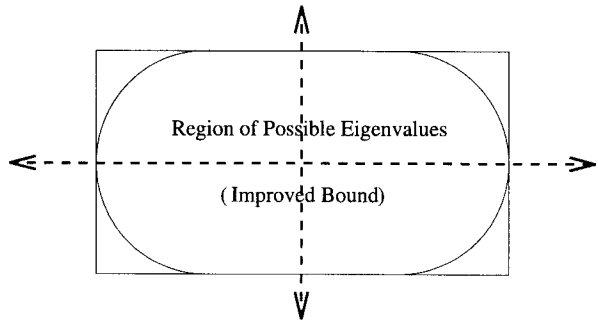

Fig. 8. Stability Boundaries in the E-plane for the Coupled Problem.

Proof. Item (i) is a simple calculation. Item (ii) follows from the Weyl theorem, which states that if **A** is self-adjoint and **B** is compact then $\sigma_{\text{ess}}(\mathbf{A}) = \sigma_{\text{ess}}(\mathbf{A}+\mathbf{B})$. Then taking **B** to be the coupling and **A** to be the uncoupled Schrödinger equation (6) proves item (ii). The third statement requires slightly more work to prove. Assume E has a non-zero complex part. Manipulating the f, g equations gives the following expression for E_{imag}:

$$2iE_{\text{imag}} \|f\|_2^2 = \int \beta F^2 g\bar{f} - \beta\bar{F}^2\bar{g}f = 2iE_{\text{imag}} \|g\|_2^2$$

Since $E_{\text{imag}} \neq 0$ by hypothesis, we conclude that $\|f\|_2^2 = \|g\|_2^2$. We henceforth assume that $\|f\|_2^2 = \|g\|_2^2 = 1$. Applying the Cauchy–Schwarz inequality gives

$$2\,|E_{\text{imag}}|\,\|f\|_2^2$$

$$\leqslant 2\int \left|\beta F^2 \|f\|\, g\right| dx \leqslant 2\,\|\beta F^2\|_\infty \|f\|_2 \|g\|_2 \qquad \text{or} \quad |E_{\text{imag}}| \leqslant \|\beta F^2\|_\infty$$

which bounds E in the infinite strip of width $\|\beta F^2\|_\infty$. The real part of E satisfies

$$E_{\text{real}} \|f\|_2^2 = -k^2 \|f\|_2^2 + \|f_x\|_2^2 + \langle f|\, V(x)\, |f\rangle$$
$$+ 2\langle f|\, \beta F^2\, |f\rangle + \tfrac{1}{2}\langle f|\, \beta F^2\, |g\rangle + \tfrac{1}{2}\langle g|\, \beta\bar{F}^2\, |f\rangle$$

where $\langle f|\, H\, |g\rangle = \int \bar{f} H g\, dx$. Our goal is to bound E_{real} from below. This, combined with the above estimate, will place the eigenvalues in a half-infinite strip. Finally the reflection symmetry we showed earlier in the section guarantees that the off axis eigenvalues lie in the intersection of the half-infinite strip and its reflection which is, of course, a rectangle.

For convenience we define $I = \int F^2 \bar{f} g\, dx$. Then the expression for E_{real} becomes

$$E_{\text{real}} = -k^2 + \|f_x\|^2 + \int |f|^2 (V(x) + 2\beta\, |F|^2)\, dx + \beta I_{\text{real}}$$

We have the following elementary inequalities:

$$\|f_x\|^2 \geqslant 0$$

$$\int V(x)\, |f|^2\, dx \geqslant V_{\min}$$

$$|\beta F^2|_{\max} \geqslant \int \beta\, |f|^2\, |F|^2 \geqslant |\beta F^2|_{\min} \qquad \beta > 0$$

$$-|\beta F^2|_{\min} \geqslant \int \beta\, |f|^2\, |F|^2 \geqslant -|\beta F^2|_{\max} \qquad \beta < 0$$

It follows from these elementary inequalities that

$$E_{\text{real}} \geqslant -k^2 + V_{\min} + 2\,|\beta F^2|_{\min} + \beta I_{\text{real}} \qquad \beta > 0$$

$$E_{\text{real}} \geqslant -k^2 + V_{\min} - 2\,|\beta F^2|_{\max} + \beta I_{\text{real}} \qquad \beta < 0$$

The value of I_{real} is trivially bounded by

$$\beta I_{\text{real}} \geqslant -|\beta I| \geqslant -\int |\beta f \bar{g} F^2| \geqslant -|\beta F^2|_{\max}$$

Therefore,

$$E_{\text{real}} \geqslant -k^2 + V_{\min} + 2\,|\beta F^2|_{\min} - |\beta F^2|_{\max} \qquad \beta > 0$$

$$E_{\text{real}} \geqslant -k^2 + V_{\min} - 3\,|\beta F^2|_{\max} \qquad \beta < 0$$

By the reflection symmetry shown earlier, or by applying the same arguments to the equation for g, we find that

$$E_{\text{real}} \leqslant k^2 - V_{\min} - 2\,|\beta F^2|_{\min} + |\beta F^2|_{\max} \qquad \beta > 0$$

$$E_{\text{real}} \leqslant k^2 - V_{\min} + 3\,|\beta F^2|_{\max} \qquad \beta < 0$$

This gives us the rectangular bound shown in Fig. 8.

This bound can be improved somewhat. In deriving this bound we have bounded the real and the imaginary parts of $I = \int F^2 \bar{f} g$ *separately* by $\int |F^2 \bar{f} g - \bar{F}^2 f \bar{g}|$. If we denote the real part of I by I_{real} and the imaginary part of I by I_{imag}, then the above arguments give

$$E_{\text{imag}} = \beta I_{\text{imag}}$$

$$E_{\text{real}} \geqslant -k^2 + V_{\min} + 2\beta\,|F|^2_{\min} + \beta I_{\text{real}} \qquad \beta > 0$$

$$E_{\text{real}} \geqslant -k^2 + V_{\min} + 2\beta\,|F|^2_{\max} + \beta I_{\text{real}} \qquad \beta < 0$$

We then use the complex Cauchy-Schwartz inequality on I

$$I = \int F^2 \bar{f} g \, dx$$

$$|I| \leqslant \|F^2\|_\infty \int |f\bar{g}| \, dx \leqslant \|F^2\|_\infty$$

$$(I_{\text{real}}^2 + I_{\text{real}}^2) \leqslant \|F^2\|_\infty^2$$

It is straightforward to check that the set of points satisfying the following inequalities

$$(I_{\text{real}}^2 + I_{\text{imag}}^2)^{1/2} \leqslant \|F^2\|_\infty$$

$$E_{\text{imag}} \leqslant \beta I_{\text{imag}}$$

$$E_{\text{real}} \geqslant -k^2 + V_{\min} + 2\beta \, |F|_{\min}^2 + |\beta| \, I_{\text{real}} \qquad \beta > 0$$

$$E_{\text{real}} \geqslant -k^2 + V_{\min} + 2\beta \, |F|_{\max}^2 - |\beta| \, I_{\text{real}} \qquad \beta < 0$$

together with reflection symmetry is the region depicted in Fig. 8, a pill shaped region made up of a rectangle together with hemicircular caps on the ends. This result is similar to the Howard semicircle theorem[21] and its various refinements, from the theory of hydrodynamic stability.

Using a result of Pego and Weinstein,[22] we can also bound the number of unstable eigenvalues in the special case where the medium is not compactly supported.

Theorem (Pego and Weinstein). Given an eigenvalue problem of the form

$$H_1 H_2 \psi = \lambda \psi$$

with H_i self-adjoint, the number of eigenvalues in the upper half plane N_{unstable} satisfies the inequality

$$N_{\text{unstable}} \leqslant d_{nd}$$

where d_{nd} is the dimension of the negative definite subspace of H_i ($i = 1$ or 2).

For eigenvalue problem (5) the factorization is accomplished through the choice

$$H_1 = \begin{pmatrix} 1 & 0 \\ 0 & -1 \end{pmatrix}$$

$$H_2 = -\partial_{xx} + \begin{pmatrix} V(x) + 2\beta |F|^2(x) - k^2 & \beta F^2(x) \\ \beta \bar{F}^2(x) & V(x) + 2\beta |F|^2(x) - k^2 \end{pmatrix}$$

This implies that the number of unstable eigenvalue is less or equal to the dimension of the negative definite subspace of H_2. We can make this bound more explicit as follows: Introduce the scalar operators $H_\pm$ defined as

$$H_- = -\partial_{xx} - k^2 + V(x) + \beta |F|^2$$

$$H_+ = -\partial_{xx} - k^2 + V(x) + 3\beta |F|^2$$

It is easy to verify that $H_- \leqslant H_2 \leqslant H_+$ for $\beta > 0$, with the inequality running in the opposite direction for $\beta < 0$. This implies that for $\beta > 0$ ($\beta < 0$) the dimension of the negative definite subspace of H_2 is less than the dimension of the negative definite subspace of $H_-(H_+)$. But $H_\pm$ is just a Schrödinger operator, and we can use any of the well known bounds on the number of bound state eigenvalues for Schrödinger operators.[23] In particular in the defocusing case when

$$\beta |F|^2 \geqslant k^2 - V(x)$$

the operator H_- is positive definite, implying that H_2 is positive definite, and thus that there are *no* instabilities. In the case where the medium is of compact support this condition cannot hold everywhere since β and $V(x)$ vanish outside of the medium. Nonetheless this is interesting in light of Shelley's observation, namely that the solution evolves so that

$$\beta |F|^2 \approx k^2 - V(x)$$

and the above condition is approximately satisfied within the support of the slab. In the focusing case ($\beta < 0$) the $|F|^2$ term in H_+ is negative definite, and the only obvious sufficient condition which will guarantee stability is to demand that

$$3\beta |F|^2 \geqslant k^2 - V(x)$$

In particular this means that $k^2 - V \leqslant 0$, so that the solution is always in a classically forbidden situation. Thus it is somewhat uninteresting from the point of view of localization.

5. NUMERICAL SOLUTION OF THE EIGENVALUE PROBLEM

In the previous section we were able to bound the region of possible instability in the complex eigenvalue plane, but were unable to establish the existence of such unstable eigenvalues analytically. We resort to direct numerical simulation to demonstrate the instability of time-harmonic solutions.

Recall that the linearized eigenvalue problem is given by

$$Ef = -k^2 f - f_{xx} + V(x) f + 2\beta |F|^2 f + \beta F^2 g$$
$$-Eg = -k^2 g - g_{xx} + V(x) g + 2\beta |F|^2 g + \beta \bar{F}^2 f$$

subject to L_2 boundary conditions. When $V(x)$, the potential, and β, the nonlinearity are both taken to be of compact support then the L_2 boundary conditions are equivalent to imposing the following boundary conditions imposed on the edge of the support:

$$\begin{aligned} f_x(0) + i(k^2 + E)^{1/2} f(0) &= 0 \\ g_x(0) - i(k^2 - E)^{1/2} g(0) &= 0 \end{aligned} \tag{7}$$

$$\begin{aligned} f_x(L) - i(k^2 + E)^{1/2} f(L) &= 0 \\ g_x(L) + i(k^2 - E)^{1/2} g(L) &= 0 \end{aligned} \tag{8}$$

These boundary conditions ensure that the free waves outside of the support of the medium decay as $x \to \pm\infty$.

We first construct F, the solution to the fixed output problem, by the numerical method outlined in Sect. 2. We then find the spectrum of the linearized problem about F in the following way: Given $E \in \mathbf{C}$ (not necessarily an eigenvalue), we use condition (7) to fix initial conditions on $f_x(0)$ and $g_x(0)$ in terms of $f(0)$ and $g(0)$ respectively. We then integrate across the medium to $x = L$. When we impose the correct boundary conditions at $x = L$ we get an equation of the form

$$\mathbf{A}(f(0), g(0))^T = \mathbf{0}$$

where $\mathbf{A} = \mathbf{A}(E, L)$ is a 2×2 matrix. Thus, $T(E) = \det \mathbf{A}$ is zero if and only if E is an eigenvalue of the linearized system. Thus the eigenvalues are computed as zeroes of the (analytic) function $T(E)$.

$T(E)$ is expensive to compute since it requires the solution of an ordinary differential equation *for each value of* $E \in \mathbf{C}$. Moreover it is not known *a priori* where these eigenvalues lie in the complex plane, except that they must satisfy the bounds derived in the previous section. For these

reasons we have found that iterative methods, such as Newton–Raphson, are too expensive to be practical, especially if we are interested in getting averaged information over many realizations of the random potential. We use instead a method based on Rouchès theorem from complex analysis, which says that given f, an analytic function of a complex variable, and Γ, a region of the complex plane, then

$$\int_{\partial\Gamma} \frac{f'(z)}{f(z)}\, dz = 2\pi i(N-P)$$

where N is the number of zeroes of f which lie inside the region Γ, P is the number of poles of f which lie in the interior of this region, and $\partial\Gamma$ denotes the boundary of Γ. To compute the zeroes of $T(E)$, we partition the complex E plane into a number of rectangles $\Gamma_{i,j}$, and calculate

$$\frac{1}{2\pi i} \int_{\partial\Gamma_{i,j}} \frac{T'(E)}{T(E)}\, dE$$

for each region $\Gamma_{i,j}$. Since $T(E)$ is entire, the contour integral counts only the number of zeros. This numerical procedure to calculated the location of eigenvalues is similar to a method used by Overman and McLaughlin[24–26] in their work on the spectrum of the scattering problem associated to the Sine–Gordon equation.

This method counts the number of eigenvalues (including multiplicities) in a region of the complex plane for a fixed realization. To calculate the density of eigenvalues in the complex plane, we simply repeat the above process for a large number of realizations, with a fixed rectangulation of the complex plane, and keep a tally of the number of eigenvalues in each rectangle.

Our implementation of this method suffers from loss of accuracy when a zero of $T(E)$ lies very near a contour $\partial\Gamma_{i,j}$, itself represented by a fixed number of grid points. In this case the integrand varies too rapidly on that portion of the contour for resolution by the fixed grid. The net effect is that when an eigenvalue lies near the boundary of one of the rectangles, it is possible for the algorithm to either miss an eigenvalue, or misplace an eigenvalue into an adjacent rectangle. To bench-mark the algorithm we conducted the following numerical experiment: We applied the algorithm to the linear function $f(z, \omega) = z - \omega$, where ω is a complex valued random variable distributed uniformly in $[-1, 1] \times [-1, 1]$. By averaging over many realizations (10,000) of the random variable we were able to compute the frequency with which the algorithm missed or misplaced an eigenvalue. We found that with thirteen grid-points on each side of the rectangle

the method missed the root entirely in roughly 5 percent of the trials, and incorrectly concluded that the root lay in an adjacent rectangle in roughly 1 percent of the trials. With twenty-seven grid-points on each side of the rectangle these errors occurred in roughly 2.5 and 0.5 percent of the trials respectively. It is worth noting that while the algorithm may occasionally misplace an eigenvalue which lies near to the contour of integration it appears to rarely find spurious eigenvalues.

5.1. Focusing Results

We have used this method to calculate the density of eigenvalues of the linearized focusing NLS eigenvalue problem. Some typical results of these experiments are shown in Fig. 9. These gray scale plots show the density of eigenvalues in the complex E plane, with white representing a large probability density and black a low probability density. These densities are based on 200 realizations of the random potential. The real axis goes from -8 to 8 and the imaginary axis from 0.1 to 2. This region has been subdivided into an 81×41 grid. The left-hand plots show the density of eigenvalues in the complex plane for random potentials of amplitude 1.0, 2.0, and 3.0 with incident wavenumber $k = 0$. The right-hand plots show the density for potentials of amplitude 1.0, 2.0 and 3.0 and incident wavenumber $k = 1$. In all cases the random potential is of length 25, a correlation length of 2, and $\beta = -1.0$. There are several general features: The first is that the eigenvalue problem has generically many complex eigenvalues, indicating that the time harmonic solutions are typically unstable. Secondly, as we would expect, the eigenvalue problems with a random potential of larger amplitude show a greater spread in the distribution of the eigenvalues. And thirdly, there is an eigenvalue "spine" along the imaginary axis, which seems to be a common feature of all the spectra.

This spine is associated with the familiar modulational instability. In the case where the support of the nonlinearity is the whole line, and where there is no random potential, there is a family of time harmonic plane-wave solutions to the focusing NLS. These plane wave solutions are always unstable, and the unstable spectrum consists of a spine along the imaginary axis whose height is proportional to the amplitude of the plane wave. This feature seems to persist even in the presence of disorder, with the height of the spine growing with the amplitude of the random potential. It has been observed previously that disorder enhances the modulational instability.[14] The heuristic reason is clear. In the fixed output problem the solutions grow as we integrate back across the support of the disordered medium. More disorder means the solutions grow faster. This means that at the front of the medium the solutions look like plane waves with comparatively

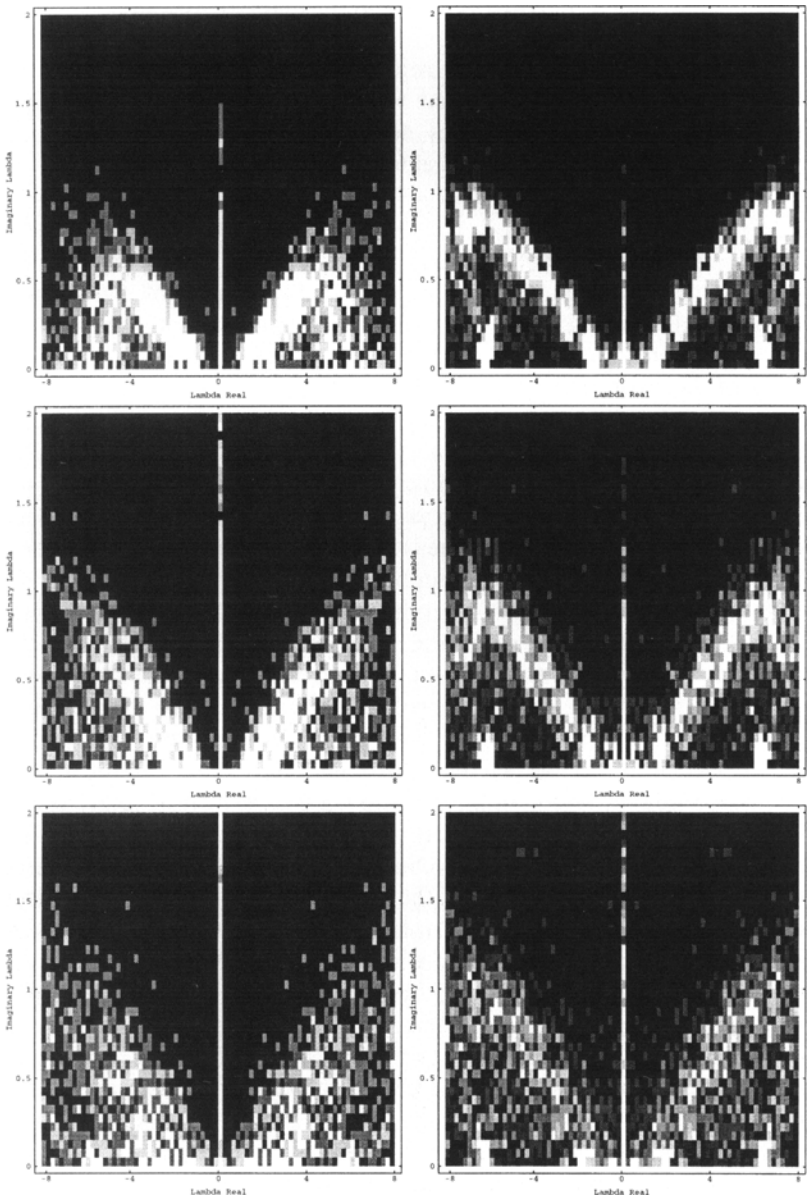

Fig. 9. Distribution of Eigenvalues—Focusing Case.

larger amplitudes, and thus the height of the spine of "modulational instability" should be comparatively larger.

5.2. Defocusing Results

Time-harmonic solutions of the cubic defocusing NLS equation,

$$k^2 F = -F_{xx} + \beta |F|^2 F + V(x, \omega) F$$

are badly behaved, and can develop singularities for finite values of x. For this reason we choose to study the time-harmonic solutions of the saturable defocusing NLS,

$$k^2 F = -F_{xx} - \frac{F}{1 + \beta |F|^2} + V(x, \omega) F \tag{9}$$

For small values of $|F|$, this equation behaves to leading order like the cubic defocusing NLS equation, but in this saturated case solutions exist for all x. We solve the associated linearized stability problem,

$$\begin{aligned} Ef &= -k^2 f + f_{xx} + V(x, \omega) f + \frac{f}{(1 + \beta |F|^2)^2} + g \frac{\beta F^2}{(1 + \beta |F|^2)^2} \\ -Eg &= -k^2 g + g_{xx} + V(x, \omega) g + \frac{g}{(1 + \beta |F|^2)^2} + f \frac{\beta \bar{F}^2}{(1 + \beta |F|^2)^2} \end{aligned} \tag{10}$$

as we did in the previous section. The length of the random medium was taken to be 50, and the correlation length of the potential was 2, so that the random medium was roughly 25 correlation lengths long. The incident wavenumber k was again taken to be 0 or 1, the amplitude of the random potential was taken to be 1.0, 2.0 or 3.0, and now $\beta = 1.0$. The results of these experiments are shown in Fig. 10. The region shown is $[-0.125, 0.125] \times [0.01, 0.15]$, subdivided into a 41×41 array of rectangles. [Note that this region of the complex plane is significantly smaller than that shown for the focusing case.]

Again we find that the time-harmonic solutions to this defocusing NLS equation are often unstable. This instability is *not* present in the absence of the potential, or in the absence of nonlinearity, and is therefore a result of the interaction of nonlinearity and randomness. In contrast, the focusing problem exhibits instability even in the absence of the random potential, and thus the instabilities present there are somewhat less surprising. It is important to note that for the parameters we have

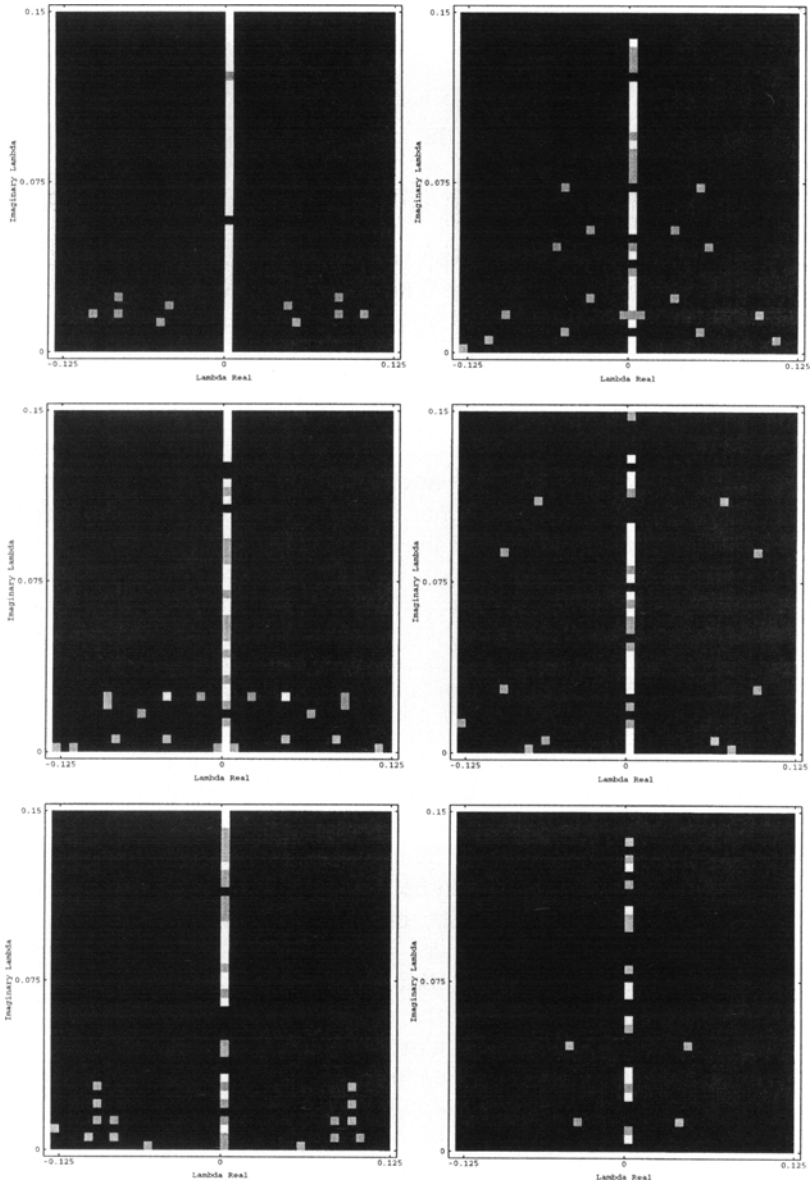

Fig. 10. Distribution of Eigenvalues—Defocusing Case.

examined, there are *significantly* fewer unstable eigenvalues in the defocusing case than in the focusing case. The average number of unstable eigenvalues in the defocusing case is roughly 0.3–0.5, while in the focusing case the average number of unstable eigenvalues is of the order of 10. In fact the instabilities for the defocusing case disappear completely for weak random potentials (potentials of small amplitude or small support). This is unsurprising, since it is known that the plane wave solutions to the defocusing NLS are stable in the absence of a potential. It is also worth noting that most of the spectrum in the defocusing case seems to be confined almost entirely to the imaginary axis. We believe that this is simply a result of the small number of eigenvalues, coupled with the symmetry of the problem. There are, on average, fewer than one eigenvalue per realization in the defocusing case. A single eigenvalue, by symmetry, must be purely imaginary. We expect, based on our numerical experiments, that potentials of larger support would have correspondingly more unstable eigenvalues, and more eigenvalues which lie off of the imaginary axis. We have done some testing of this hypothesis with a modification of the code described above which simply counts the number of unstable eigenvalues. The results of some experiments run using this code are illustrated in Fig. 11, which depicts the average number of unstable eigenvalues (based on 200 realizations of the random potential) as a function of the support of the length of the disordered medium. The average number of unstable eigenvalues is seen to grow with the length of the disordered medium. Intuitive arguments suggest that the number of eigenvalues should grow linearly with the length of the medium, which appears consistent with the graph in Fig. 11.

We also note that while there is a spine of spectrum in both the defocusing and the focusing cases, there are qualitative differences. In the

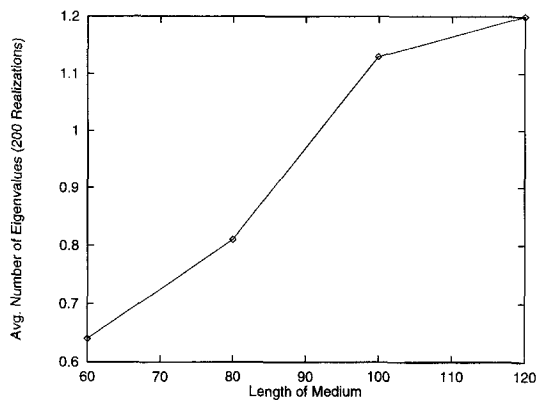

Fig. 11. Average Number of Eigenvalues vs. Length of Medium.

focusing case the height of this spine is observed to grow linearly with the amplitude of the random potential, while in the defocusing case, the height of this spine appears to be largely independent of this amplitude.

Finally, we would like to mention the bounds derived in the previous section. We have not included these bounds in the previous graphs, since they depend on the time-harmonic solution F, and so are realization dependent. However for a single realization it is easy to verify that all of the eigenvalues we find lie within these bounds. In the defocusing case in particular these bounds appear to be far from tight. This is to be expected since in the case where the random potential vanishes there are no instabilities, but the bounds we derived do not generally vanish.

5.3. Resonances and Instabilities

It is not difficult to understand heuristically the origin of unstable eigenvalues. As we remarked earlier, the eigenvalue problem in Eq. (5) looks very similar to the pair of second order Schrödinger eigenvalue problems given by

$$\begin{aligned} Ef &= -k^2 f - f_{xx} + V(x)\, f + 2\beta\, |F|^2 f \\ -Eg &= -k^2 g - g_{xx} + V(x)\, g + 2\beta\, |F|^2\, g \end{aligned} \tag{11}$$

but is complicated by the presence of a skew-adjoint coupling. It is convenient to introduce an artificial coupling constant λ for the non-self-adjoint part of the eigenvalue problem

$$\begin{aligned} Ef &= -k^2 f - f_{xx} + V(x)\, f + 2\beta\, |F|^2 f + \lambda\beta F^2 g \\ -Eg &= -k^2 g - g_{xx} + V(x)\, g + 2\beta\, |F|^2\, g + \lambda\beta \bar{F}^2 f \end{aligned} \tag{12}$$

Again, when $\lambda = 0$ the eigenvalue problem is self-adjoint and the spectrum is as given before—the entire real axis is continuous spectrum, of multiplicity two in $(-\infty, -k) \cup (k, \infty)$ and multiplicity 4 in $[-k, k]$. Also there is the possibility of having imbedded eigenvalues in $(-\infty, -k) \cup (k, \infty)$.

It is obvious that any eigenvalues of the $\lambda = 0$ problem can potentially move into the complex plane as the coupling is increased, and become unstable eigenvalues. What is not so obvious is that there are eigenvalues in the finite λ case which do not correspond to any eigenvalues in the $\lambda = 0$ case, but instead arise from resonances, or second sheet poles, of the resolvent operator in the $\lambda = 0$ problem. This sort of "bifurcation" is unique to infinite dimensional problems, since in finite dimensional systems the analytic continuation of an eigenvalue is itself an eigenvalue. (Similar

mechanisms for the onset of instability have been observed, for example, by Pego and Weinstein in the study of the stability of travelling wave solutions to the generalized KdV equation,[22] and by Bourlioux, Majda, and Roytburd[27] in the study of combustion.)

We have numerically documented these resonances crossing the branch cut on the real axis, and becoming eigenvalues as the coupling constant λ is varied. We used a standard shooting method to find a single unstable eigenvalue. The value of the coupling was decreased, and the eigenvalue calculated again using the old eigenvalue/eigenvector as the initial guess for the shooting method. Convergence of the shooting method was rapid, since only small changes were made in the coupling constant. These experiments were run with a piecewise constant potential, like that considered by Devillard and Souillard.

Figure 12 illustrates the path of a single eigenvalue of the focusing problem as the coupling constant λ is varied between 0 and 1. That end of the path which lies below the real axis, where the "eigenvalue" is actually a resonance, corresponds to $\lambda = 0$, while that end which lies above the real axis, where the eigenvalue is a true eigenvalue, corresponds to $\lambda = 1$.

Figure 13 shows the f and g eigenfunctions for the fully coupled case, and the effective potential $V(x) + 2\beta |F|^2$ of the uncoupled problem. Generically one member of the (f, g) pair has most of its mass supported near a well of the effective potential $V(x) + 2\beta |F|^2 (x)$. This is consistent with the interpretation of these complex eigenvalues as being connected with the phenomena of resonance. Since the spectrum in the $\lambda = 0$ case is the union of the f spectrum and the g spectrum these resonance poles are generically associated with either f or g. In the case shown in Fig. 13, g (the

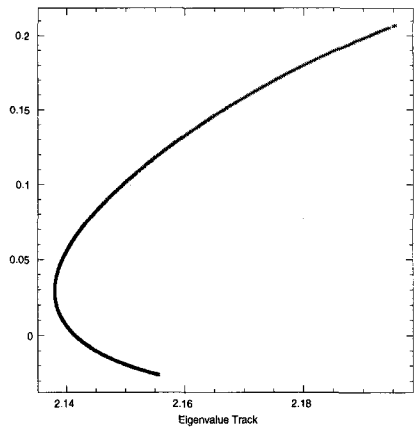

Fig. 12. Eigenvalue Path in Complex Plane for $\lambda \in [0, 1]$.

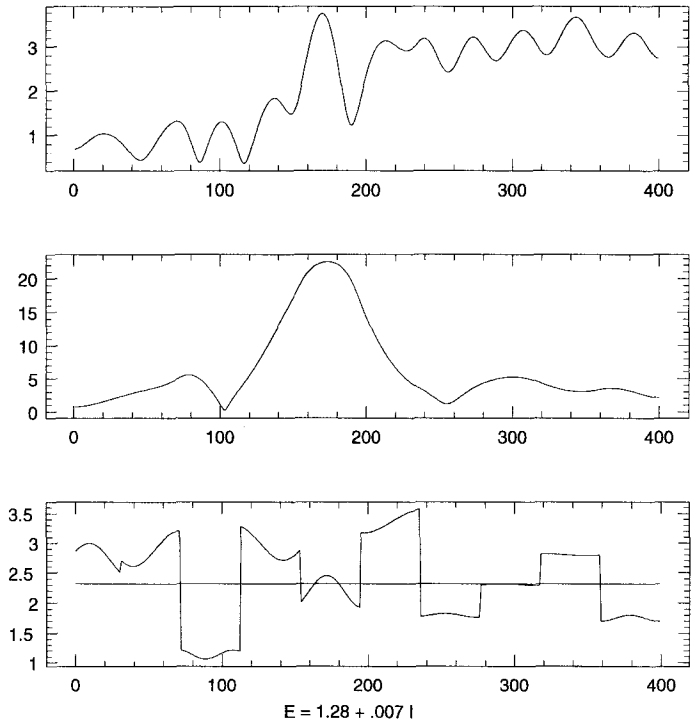

Fig. 13. The f and g Eigenvectors, and the Effective Potential.

middle graph) happens to be the resonant member of the pair. There is an second eigenvalue at $-\bar{E}$ where f is the resonant member of the pair. Also note that within the medium the amplitude of g, the resonant member of the pair, is much greater than the amplitude of f (the upper graph), the nonresonant member of the pair.

This interpretation of the nature of the instabilities of the time-harmonic solutions of the random NLS equation suggests a heuristic interpretation of the numerical observations of Shelley. The instabilities are associated with resonances of a scattering problem with effective potential $V(x)+2\beta\,|F|^2\,(x)$. These resonant eigenfunctions are supported near local minima of the effective potential $V(x)+2\beta\,|F|^2\,(x)$. The instability causes growth of the unstable modes. In the focusing case ($\beta<0$) this growth causes the minima to become deeper. This causes a greater instability, which causes the minima to become deeper still. This process continues until the effects of diffraction become important. In the defocusing case, the initial instability causes growth in the solution, which is supported near local minima of the effective potential $V(x)+2\beta\,|F|^2\,(x)$. However, the

evolution proceeds very differently than in the focusing case. Growth in the solution near a local minima causes the minima to become less deep. This causes less instability. Thus the effect of the instability in the defocusing case is to fill in the minima and eliminate the source of the instability.

6. ASYMPTOTICS

In their numerical simulations, Shelley, Caputo, and Newell,[9] and Shelley[18] observed that at long times the focusing case tended to look like a large number of solitons bound to local minima of the potential, while in the defocusing case Shelley[18] observed that the wavefunction was "slaved" to the effective potential. It is interesting to ask whether it is possible to construct solutions of the NLS in the presence of a potential which at least approximately match these observations. In this section we discuss such constructions.

There are a number of papers which construct solutions to the focusing NLS equation in the semiclassical limit (limit of small dispersion) in the presence of a potential. These solutions consist of solitons which are bound to critical points of the potential. [Note that these critical points may be maxima or minima.] The most general construction is due to Oh.[28] Given a potential with N critical points he is able to construct 2^N solutions, corresponding to the presence or absence of a soliton at each critical point. More details can be found in Refs. (29, 28, 30).

The observed defocusing solution, $\beta |F|^2 \approx k^2 - V(x)$, is obviously not an exact solution of the defocusing random NLS equation, but can be found asymptotically as a solution in the semi-classical limit of large incident wavenumber or (equivalently) slowly varying $V(x)$. This is seen most easily by introducing the formal expansion parameter ε

$$i\varepsilon\psi_t = -\varepsilon^2\psi_{xx} + V(x)\,\psi + \beta\,|\psi|^2\,\psi$$

where the limit $\varepsilon \to 0$ corresponds to $k \to \infty$. Making the geometrical optics Ansatz

$$\psi = A(x, t)\exp(iS(x, t)/\varepsilon)$$

and collecting powers of ε, gives the eikonal and transport equations

$$-S_t = S_x^2 + V(x) + \beta A^2$$

$$A_t = 2S_x A_x + S_{xx} A$$

The first of these equations (eikonal) involves both the amplitude and the phase because of the strongly nonlinear character of the problem. (In semi-classical theory of the linear Schrödinger equation, the eikonal equation involves only the phase.) The second equation (transport) is identical in the linear and nonlinear cases, as can be seen by the lack of explicit β dependence. In general these equations exhibit all of the phenomena associated with nonlinear hyperbolic systems (shock formation, caustics, etc.) and are extremely difficult to solve. However since we are interested in monochromatic solutions, we can further require that

$$S_t = -k^2$$

$$A_t = 0$$

which gives us the two relations

$$S_x^2 = k^2 - V - \beta A^2 \tag{13}$$

$$\frac{S_{xx}}{S_x} = -2\frac{A_x}{A} \tag{14}$$

The eikonal relationship ($S_x^2 = k^2 - V - \beta A^2$) basically represents conservation of energy in the semi-classical picture. The kinetic energy S_x^2 is equal to the total energy k^2 minus the potential energy. The potential energy is in two parts. The first part $V(x)$ is due to the external potential, while the second part is due to the nonlinear self-interaction βA^2.

The transport equation (14) can be integrated to obtain

$$S_x = \frac{c}{A^2}, \qquad \text{or} \quad A = \frac{c'}{S_x^{1/2}} \tag{15}$$

Comment: The same transport equation arises in classical WKB theory, where the WKB solution of the linear problem is given by

$$\psi_{\text{linear}}^{WKB} = \frac{\exp(iS(x,t)/\varepsilon)}{\sqrt{S_x}}$$

$$S_x^2 = k^2 - V(x)$$

This is not surprising since the transport equation represents a semi-classical conservation of particle number in the same way that the eikonal equation represents a conservation of energy. The derivative of phase S_x represents a local particle velocity in the semiclassical picture. In order that the flux of particles through the point x remains constant, it is necessary

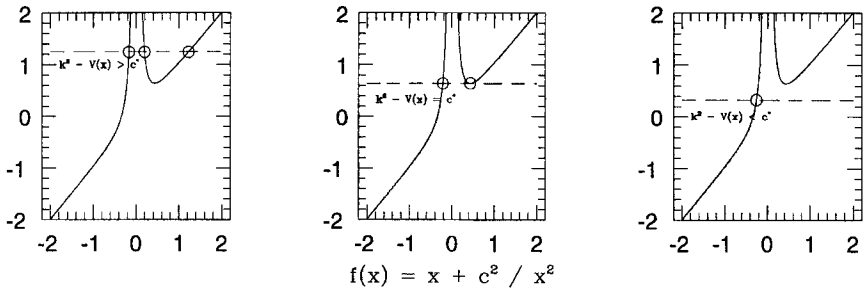

Fig. 14. The subcritical, critical, and supercritical values of c^*.

to require that the density of particles at x must be proportional to S_x^{-1}. Since the particle density is given by $\rho = |\psi|^2$ it follows that the amplitude must be proportional to $S_x^{-1/2}$. This conservation of particle number is clearly unaffected by the self-interaction represented by the nonlinearity

The transport equation (15) can be used to eliminate the phase from Eq. (13), and we are left with an algebraic equation which depends upon a constant of integration c:

$$\beta A^6 + c^2 - (k^2 - V(x))\, A^4 = 0 \tag{16}$$

This polynomial has four real roots and two imaginary roots when

$$k^2 - V(x) \geqslant 3\left(\frac{\beta c}{2}\right)^{2/3} \tag{17}$$

and 6 complex roots when this condition is violated. The easiest way to see this is to look at the equivalent equation

$$k^2 - V = \beta y + \frac{c^2}{y^2} = f(y)$$

where $y = |A|^2$. For $y > 0$ the function $f(y)$ is positive with a local minima at $y_0 = (2c^2/\beta)^{1/3}$, $f(y_0) = 3(\beta c/2)^{2/3}$. If $k^2 - V(x) \leqslant 3(\beta c/2)^{2/3}$ then the only real root occurs for $y < 0$, corresponding to imaginary A. In the case $k^2 - V(x) \leqslant 3(\beta c/2)^{2/3}$ there are two positive roots and one negative root for y, corresponding to four real roots and two imaginary roots for $|A|$. This is illustrated in Fig. 14.

It is useful to examine the limiting cases $\beta \to 0$ and $\beta \to \infty$, and to note a few properties. In the first case, for $0 < \beta \ll 1$, we find that

$$A \approx c^{1/2}(k^2 - V(x))^{-1/4} + O(\beta)$$

while for $\beta \gg 1$ we find

$$A^2 \approx \frac{k^2 - V(x)}{\beta} + O(\beta^{-2})$$

Note that $A^2 = k^2 - V(x)/\beta$ is *exactly* a root when $c = 0$. These two limits represent the two branches of solutions to Eq. (16). In the limiting case $\beta \approx 0$ the smaller root persists while the larger root moves off towards infinity. In the other limiting case, $\beta \gg 1$ the smaller root moves towards $x = 0$ while the larger root stays fixed. Thus the inner branch, which has smaller amplitude, is in some sense a "near-linear" solution while the outer branch is a strongly nonlinear solution. We suspect (but have no rigorous proof) that the outer branch—Shelley's observed asymptotic time-harmonic solution—is dynamically stable while the inner branch is not.

Physically the constant c represents the momentum of the wave inside the medium, and condition (17) simply says that in order to support propagating solutions the wave must have sufficient energy to overcome the potential barrier. In fact when $\beta = 0$, Eq. (17) is simply the (semi-) classical condition $k^2 - V(x) > 0$. Thus Eq. (17) should be thought of as an extension of this result to the nonlinear case

It is also worth noticing that, given $A_c(x)$, a root of Eq. (16) for a given value of the integration constant c, we have

$$|c| < |c'| \to A_c(x) > A_{c'}(x)$$

and in particular

$$\beta A_c^2(x) \leqslant k^2 - V(x)$$

with equality iff $c = 0$. In Section 4, we found the sufficient condition for stability of a time-harmonic solution:

$$\beta |F|^2 \geqslant k^2 - V(x)$$

This condition is violated by every solution with $c \neq 0$. It seems plausible then that most of these solutions are unstable and are not observable in practice. Since this condition has only been shown to be sufficient, and not necessary, we have as yet no proof of this expectation.

7. CONCLUSION

We have studied the NLS equation with a random potential. Our methods have been primarily numerical, but with some use of mathematical and asymptotic analysis. Our primary goal is to understand the

competition between nonlinearity and randomness in regard to the striking physical phenomenum of "localization".

The problem which we are primarily interested in is the time-dependent scattering problem, where we consider the long time state of a plane wave incident on a disordered medium. In contrast Devillard and Souillard[10] and Papanicolaou *et al.*[11, 17] studied the time-independent scattering problem in the fixed output and fixed input formulations, and Fröhlich, Spencer and Wayne[13] studied the time-dependent initial value problem. Note that in the absence of nonlinearity these problems are all, in some sense, the same. This is no longer true, however, in the nonlinear problem.

The phenomena which arise in the time dependent scattering problem are perhaps best described by Figs. 5a, b, and c, which display typical realizations of a wave in a random slab. These realizations show the distinct behavior of the wave in linear, focusing, and defocusing random media. In the three cases the waves possess very different "localization features"—exponential localization in the linear case; in focusing nonlinearities, solitary waves locked to local minima; the approach to a time-harmonic wave by a "semiclassical filling in process" in the case of defocusing nonlinearity.

We show that time-harmonic solutions to random NLS are typically unstable; thus suggesting that earlier studies of time-harmonic localization for a fixed output problem are of limited relevance to the time dependent scattering problem. We have derived analytically bounds on the locations of the unstable eigenvalues. Numerically, we have shown that unstable eigenvalues indeed exist; moreover, we have computed some intriguing distributions of these unstable eigenvalues. These distributions are distinctly different in the focusing and defocusing cases. We have interpreted these instabilities in terms of resonances in the associated linearized problem. In addition, we note that since these unstable eigenfunctions tend to be supported at critical points of the potential, which themselves are distributed throughout the entire medium, the effect of these instabilities is against localization. Finally, in the defocusing case, we develop a semi-classical argument to describe the "filling in process" toward a stable (but atypical) time-harmonic wave as observed in the numerical experiments.

In the focusing case we have seen that the long time wavefunction appears to consist of a large number of soliton-like structures which are bound to local minima of the potential. The numerical experiments seem to indicate that these soliton-like structures can arise anywhere within the medium, and the amplitudes of these structures do not appear to decay with distance into the medium. Therefore we conjecture that in the case of a semi-infinite medium, for sufficiently long times the wavefunction will have mass located arbitrarily far into the medium. In the defocusing case

we have seen that the long time state of the wavefunction "mimics" the imposed external potential. Note that both of these effects appear to be a consequence of the fact that the incident plane wave has infinite mass. In both cases the apparent limiting states have infinite L_2 norm. Since the NLS equation conserves L_2 norm these solutions cannot evolve from an initial condition with finite L_2 norm. Thus these conjectures do not contradict those by Frölich, Spencer, and Wayne, where they conjecture that the NLS initial value problem localizes for L_2 initial data.

We close by mentioning several possible new directions: First, it would be interesting to understand the nature and origin of the fine structure in the k dependence of the reflection coefficients. Precise characterizations of localization in the nonlinear case, as well as equivalences between different definitions, are needed. In the case of spatially localized initial data, can localization be characterized in terms of bounded (or slow growth) of the variance? With such a characterization, can rigorous mathematical arguments be given which establish the presence or absence of localization?

ACKNOWLEDGMENTS

We would like to thank the referee for his constructive and insightful comments, which improved the presentation of this paper. This work was funded in part by, NSF DMS 9407473 to J.C.B., AFOSR-90-0161 and NSF DMS 8922717 A01 to D.W.M., and NSF DMS 9396403 (PYI) and 9404554 and DOE DE-FG02-88ER25053 to M.J.S.

REFERENCES

1. P. W. Anderson, Absence of Diffusion in Certain Random Lattices, *Phys. Rev.* **109**:1492 (1958).
2. J. Fröhlich and T. Spencer, Absence of diffusion in the Anderson tight binding model for large disorder or low energy, *Comm. Math. Phys.* **88**:151–184 (1983..
3. F. Martinelli and E. Scoppola, Remark on the absence of absolutely continuous spectrum for d-dimensional Schrödinger operator with random potential for large disorder or low energy, *Comm. Math. Phys.* **97**:465–471 (1985).
4. S. Molchanov and M. Aizenmann, Localization for Large Energy/Disorder: Elementary Derivation. Preprint (1993).
5. R. Carmona and Lacroix, *Spectral Theory of Random Schrödinger Operators*, Probability and its Applications (Birkhauser, 1990).
6. L. Pastur and A. Figotin, *Spectra of Random and Almost Periodic Operators* (Springer-Verlag, 1992).
7. B. Derrida and E. Gardner, Lyapunov Exponent of the One Dimensional Anderson Model, *J. Physique* **45**:15–21 (1984).
8. B. Doucot and R. Rammal, Invariant Imbedding approach to Localization I,II, *J. Physique* **48**:509 (1987)

9. M. Shelley J. Caputo, and A. Newell, Nonlinear Wave Propagation through a Random Medium and Soliton Tunneling, *Proceedings on the Conference on Non-integrability, Ile D'Oleron*, pp. 49–64, 1988.
10. B. Souillard and P. Devillard, Polynomially Decaying Transmission for the Nonlinear Schrödinger Equation in a Random Medium, *J. Stat. Phys.* **43**:423–439 (1986).
11. B. White R. Knapp, and G. Papanicolaou, Transmission of Waves by a Nonlinear Medium, *J. Stat. Phys.* **63**(4):567-584 (1991).
12. B. Doucot and R. Rammal, On Anderson Localization in a Nonlinear Random Medium, *Europhys. Lett.* **3**:969 (1987).
13. T. Spencer J. Fröhlich, and C. E. Wayne, Localization in Disordered, Nonlinear Dynamical Systems, *J. Stat. Phys.* **42**:247 (1986).
14. S. A. Gredeskul and Y. S. Kivshar, Propagation and Scattering of Nonlinear Waves in Disordered Systems, *Physics Report* **216**(1):1–61 (1992).
15. S. He and J. D. Maynard, Detailed Measurements of Inelastic Scattering in Anderson Localization, *Phys. Rev. Lett.* **57**(25):3171-3174 (1986).
16. J. Bronski, *Aspects of Randomness in Nonlinear Wave Propagation*, Thesis (Princeton University, 1994).
17. R. Knapp G. Papanicolaou, and B. White, Nonlinearity and Localization in One Dimensional Random Media, In *Disorder and Nonlinearity*, pp. 2–26.
18. M. J. Shelley, Wave Propagation in the Random NLS Equation, in preparation (1994).
19. V. I. Oseledec, A Multiplicative Ergodic Theorem: Lyapunov Characteristic Numbers for Dynamical Systems, *Trans. Moscow Math. Soc.* **19**:197–231 (1968).
20. M. Ablowitz and J. Ladik, Non-linear Differential-Difference Equations and Fourier Analysis, *J. Math. Phys.* **17**:1011 (1976).
21. P. G. Drazin and W. H. Reid, *Hydrodynamic Stability*, Cambridge Monographs on Mechanics and Applied Mathematics (Cambridge University Press, New York, 1981).
22. R. Pego and M. Weinstein, Eigenvalues, and Instabilities of Solitary Waves, *Phil. Trans. R. Soc. Lond.* **A340**:47–94 (1992).
23. M. C. Reed and B. Simon, *Methods of Modern Mathematical Physics* (Academic Press, New York, 1980).
24. A. R. Bishop, D. W. McLaughlin, and E. A. Overman II, Coherence and Chaos in the Driven Damped Sine Gordon Equation, *Physica D.* **19** (1986).
25. A. R. Bishop, M. G. Forest, D. W. McLaughlin, and E. A. Overman II, A Quasiperiodic Route to Chaos in a Near Integrable PDE, *Physica D.* **23**:293 (1986).
26. D. W. McLaughlin and E. A. Overman II, Whiskered Tori for Integrable Pde's; Chaotic Behavior in Near Integrable Pde's, *Surveys in Applied Math.* **1**:83–200 (1995).
27. A. Bourlioux, A. Majda, and V. Roytburd, Theoretical and Numerical Structure for Unstable One-Dimensional Detonations, *SIAM J. Appl. Math.* **51**(2):303 (1991).
28. Y. G. Oh, On Positive Multi-Lump Bound States of NLS Equations Under Multiple Well Potential, *Comm. Math. Phys.* **131**:223–253 (1990).
29. A. Floer and A. Weinstein, Nonspreading Wave Packets for the Cubic Schroedinger Equation with a Bounded Potential, *Journal of Functional Analysis* **69**:397–408 (1986).
30. M. Rose and M. Weinstein, On the Bound States of the NLS Equation with a Linear Potential, *Physica D* **30**:207–218 (1988).